Magnetization reversal and soft modes in nanorings: Transitions between onion and vortex states studied by Brillouin light scattering

F. Montoncello,[1] L. Giovannini,[1] F. Nizzoli,[1] H. Tanigawa,[2] T. Ono,[2] G. Gubbiotti,[3] M. Madami,[3] S. Tacchi,[3] and G. Carlotti[3,4]

[1]*Dipartimento di Fisica, Università di Ferrara and CNISM, Via Saragat 1, I-44100 Ferrara, Italy*

[2]*Institute for Chemical Research, Kyoto University, Uji, Kyoto 611-0011, Japan*

[3]*CNISM, Dipartimento di Fisica, Università di Perugia, Via A. Pascoli, I-06123 Perugia, Italy*

[4]*Research Center INFM-CNR S3, I-44100 Modena, Italy*

(Received 30 April 2008; revised manuscript received 4 July 2008; published 26 September 2008)

We present a joint experimental and theoretical investigation of the magnetization reversal process in an array of circular permalloy nanorings. The longitudinal hysteresis loop measured by magneto-optic Kerr effect exhibits the typical two-step switching behavior corresponding to transition from the onion to the vortex state and vice versa with plateaux in each loop branch. The frequencies of the spin excitations in these configurations calculated by means of the dynamical matrix approach are in good agreement with those measured by Brillouin light scattering. Several types of spin modes are found localized in different regions of the rings. It is found that the onion-to-vortex and the vortex-to-onion transitions are triggered by soft spin modes. The shape and symmetry of the dynamic magnetization profile of these soft modes provide the initial modifications of the magnetization at the onset of the transitions.

DOI: 10.1103/PhysRevB.78.104421 PACS number(s): 75.40.Gb, 75.30.Ds, 75.75.+a, 78.35.+c

I. INTRODUCTION

Brillouin light scattering (BLS) is the ideal technique for measuring thermally excited spin-wave modes in laterally confined magnetic structures.[1] In particular with BLS it is possible to detect within a single measurement several discrete spin modes produced by lack of translation invariance in the sample plane (lateral confinement) and by the inhomogeneity of the internal magnetic field as well.[2] In this context, ring shape elements exhibit a particularly rich spectrum of magnetic excitations[3–10] associated with the different magnetic ground state of the system, namely, the vortex state in which the magnetization is circumferential to the ring without stray fields, and the so-called "onion" state with two opposite head-on-head domain walls.[11]

In a recent Letter[8] we presented a spin dynamic study of the magnon modes of a magnetic ring in the vortex state with special emphasis on the frequency splitting of both radial and azimuthal modes induced by an applied magnetic field.

In the present paper we mainly focus our attention on the investigation of the role played by magnetic excitations in assisting and driving the magnetization reversal process during the onion-to-vortex transition (and vice versa) in circular nanorings. It has been recently shown[12–14] that when an abrupt magnetization switching occurs in a nanoelement it is accompanied by a soft magnetic mode (its frequency goes to zero). Furthermore, the spatial symmetry of the soft mode determines the initial steps (onset) of the microscopic reversal path. The spectra of thermally excited spin excitations have been detected with BLS, and the recently developed dynamical matrix method (DMM) (Refs. 15–17) has been used to calculate both eigenvalues (mode frequencies) and eigenvectors (mode profiles) directly in the frequency domain without the need of integrating the Landau-Lifshitz equation and Fourier transforming the time evolution of the magnetization. The comparison between the measured BLS spectra and the calculated mode frequencies and scattering intensities of each mode allows us to recognize the physical characters of the modes in terms of spatial distribution of the dynamical magnetization, of localization regions, and of the number of nodal surfaces. We consider the evolution of the spin excitations as a function of the static magnetic field from negative to positive values and encompassing the different magnetic ground states of the rings including the onion, the vortex, and the reversed-onion states. The aim of this paper is to achieve an exhaustive comprehension of the processes that trigger the magnetization phase transition. In Sec. II we briefly describe the samples preparation procedure and the experimental details. The BLS results are shown in Sec. III together with the calculations. Conclusions are drawn in Sec. IV.

II. MAGNETIC CHARACTERIZATION OF SAMPLES

A squared array of 20-nm-thick ring-shaped dots of Permalloy ($Ni_{80}Fe_{20}$) was fabricated by a combination of *e*-beam lithography, *e*-beam evaporation, and lift-off processes.[16] The rings have outer radius $R=355$ nm and width $w=200$ nm. A separation among the rings of 330 nm is large enough to consider the rings to a good approximation as noninteracting. The longitudinal hysteresis loop measured by magneto-optic Kerr magnetometry (MOKE) is shown in Fig. 1 together with the reference frame adopted in this paper. The ring lies in the x-y plane, the z axis is normal to the surface, and a magnetic field was applied in the sample plane along the y direction. The x axis is defined by the polar angle $\phi=0$ and the y axis by the angle $\phi=\pi/2$.

The model ring employed in both static and dynamic simulations has outer radius equal to 336 nm, internal radius 156 nm, and thickness 20 nm. The cell size of the micromagnetic calculations is $6\times6\times20$ nm^3.[18] Micromagnetic simulations demonstrated[11] that in axially symmetric circular

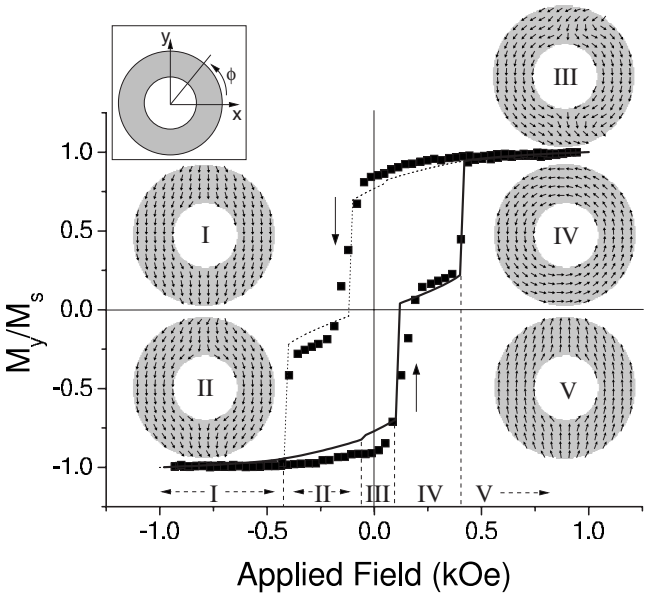

FIG. 1. Experimental longitudinal Kerr hysteresis loop (symbols). Calculated loop in the micromagnetic approach: solid line refers to increasing applied field, dotted line to decreasing field. M_y/M_s is the component of the magnetization in the direction of the applied field in unit of the saturation magnetization M_s. Five configurations of the equilibrium magnetization are sketched and labeled by Roman numbers: onion state (phase I), distorted onion states (II and III), vortex state (IV), and reversed-onion state (V). The inset shows the reference system.

ring, the vortex state is not obtained and the loop is characterized by a single transition from the onion to the reversed-onion state. On the contrary, when the axial symmetry of the ring is broken, the vortex nucleation is achieved and realistic values of the critical fields are obtained. In this paper we have adopted such approach by right shifting the hollow of one cell (6 nm) from the center. This symmetry breaking introduced in the calculations simulates the irregularities present in the real rings. Although the asymmetric ring (AR) has lost the inversion symmetry together with the axial symmetry, it possesses a mirror plane (the x-z plane) also in the presence of an external field applied along the y axis. Therefore, also the magnetization exhibits such symmetry element (the mirror plane). The parameters used in the calculations are: saturation magnetization M_s=750 G, gyromagnetic ratio γ=2.95 GHz/kOe, and exchange stiffness $A=1\times10^{-6}$ erg/cm. The magnetization equilibrium states have been calculated by means of the object-oriented micromagnetic framework OOMMF (Ref. 19) for each value of the field H. These equilibrium states have been used for simulating the hysteresis loop and for computing the excitations with the DMM (in the zero-temperature approximation).As it can be seen in Fig. 1, the experimental Kerr loop is well reproduced by the micromagnetic simulation. Starting from $H=-1.0$ kOe, the magnetization decreases slightly with increasing field up to about +110 Oe. In this region, the calculations give three kinds of distinct equilibrium states as it can be seen in insets of Fig. 1: state I, slightly distorted onion state due to the shifted hollow from large negative fields up to −431 Oe; state II, a further distorted onion state with the appearance of curling magnetization in the range (−430, −48) Oe; and state III, a strongly distorted state in the range (−47, +110) Oe with the magnetic moments on top and bottom of the ring lying almost horizontally and a more pronounced curling magnetization on the outer border for $\phi \approx \pm \pi/3$. The transitions at $H=-430$ and −48 Oe produce small discontinuities in the calculated cycle of Fig. 1, and they are classified as first-order transitions. We believe that this is an artifact due to the serrated shape of the borders of the ring used in the simulation; whereas in the ideal case of perfectly circular borders, no discontinuity is actually expected. Moreover, measurements on arrays of rings wash out such small jumps as it appears in the experimental Kerr loop of Fig. 1.

As the magnetic field is reversed and increased to positive values, two abrupt jumps are present in the hysteresis loops at critical fields $H_{c1}\approx110$ Oe and $H_{c2}\approx417$ Oe, which correspond to the vortex nucleation and annihilation, respectively. The magnetization plateau (which is about 300 Oe wide) observed when $H_{c1}<H<H_{c2}$ corresponds to the configuration where the vortex state is stable (state IV). For $H>H_{c2}$ the magnetization turns to the reversed-onion state (state V) and points upward. We will focus our investigation on the main transitions corresponding to the two large discontinuities in the Kerr loop, i.e., state III→state IV (onion-to-vortex transition) and state IV→state V (vortex-to-reversed-onion transition).

As already remarked, the x-z plane is a mirror plane for the system; therefore the magnetization, which is an axial vector, is invariant for reflections about the mirror plane followed by a change of sign. In other words, the x and z components of the magnetization are odd and the y component is even for such symmetry operation. It can be verified that the equilibrium states shown in Fig. 1 exhibit such behavior. As a consequence of the symmetry of the equilibrium states, the spin excitations, which are eigenvectors of the dynamical problem, may be either symmetric (S) or antisymmetric (AS) with respect to the mirror plane. Although strictly speaking S and AS apply to the symmetry of modes under inversion operation, in this paper we adopt this definition for the mirror operation referred to the x and z components of the dynamic magnetization, which behave similarly.

III. BRILLOUIN SCATTERING RESULTS AND SPIN MODE CALCULATIONS

Brillouin light-scattering experiments were performed in the backscattering configuration using a Sandercock-type (3+3) tandem Fabry-Perot interferometer.[20] The x-z incidence plane of light was perpendicular to the applied magnetic field H. The frequencies of the spin excitations extracted from the measured BLS spectra are shown in Fig. 2. The spectra were recorded at a 40° incidence angle of light with respect to the sample normal starting from −600 up to 600 Oe of applied field encompassing the initial onion state, the vortex, and eventually the reversed-onion state. The two critical fields H_{c1} and H_{c2} already observed in the Kerr loop correspond to discontinuities in the mode experimental dispersion vs H as shown in Fig. 2. With respect to the previous

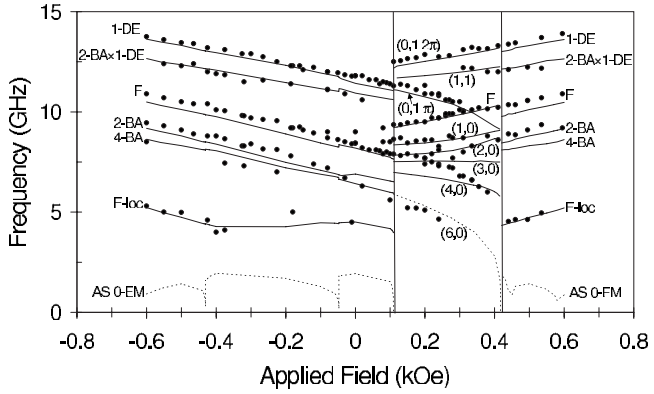

FIG. 2. BLS measured frequencies of the spin modes (symbols) starting from negative to positive applied field values. The calculated frequency dispersions of the modes (lines) are labeled according to the character of the modes. (m,n) are vortex modes. DE, BA, F, and EM are Damon-Eshbach-type, backwardlike, fundamental, and end modes, respectively. The two thin vertical lines mark the critical fields $H_{c1}=110$ Oe (onion-to-vortex transition) and $H_{c2}=417$ Oe (vortex-to-onion transition).

Letter,[8] where the system at remanence was demagnetized and the rings were in the vortex state, in the present case the different magnetic history of the sample gives rise in the neighborhood of $H=0$ to the onion state, which persists until $H=110$ Oe.

In Fig. 2, the experimental data are shown and compared with the frequencies calculated with the DMM. In general, the agreement between the measured and calculated mode frequencies is quite good. In this figure, we show a few modes allowed by the BLS selection rules[21] having the smallest number of nodal surfaces and the largest cross section. Other modes are not presented to avoid overcrowding. In addition, the dashed lines indicate modes that exhibit a tendency to soften in proximity of the critical fields. In the following we discuss separately the modes of the two magnetic phases characterized by the onion and vortex states, respectively. In order to indicate the region of localization of the spin modes in the vortex state, we use the angle ϕ. In particular we label the modes localized in the two arms of the ring parallel to the y axis by π (left arm) and 2π (right arm) according to the values taken by the angle ϕ in the center of the arms. The same nomenclature was used in Ref. 8.

From the experimental point of view, we point out that the BLS data presented in this paper differ from those already shown in the previous work[8] because of the different magnetic ground state in zero applied field (onion instead of vortex) caused by the different magnetic history. As far as the calculated curves are concerned, we remark that in the present case, the hollow of the ring is shifted differently from previous works.[8,22] Apart from the lowest modes near the critical fields, labeled (6,0) and AS 0-EM, this fact however produces only small changes in the mode frequencies so that the general interpretation of the spectra is unchanged.

A. Onion state

When the rings are in the onion state there are essentially two families of modes. (i) "Bulk" modes mainly localized in both the ring arms parallel to the direction of the applied field ($\phi\approx\pi$ and 2π), where the internal field defined as the sum of the Zeeman and demagnetizing fields is approximately uniform and equal to the value of the external field H. These modes resemble those existing in a magnetic stripe magnetized parallel to its length and having width equal to the ring width, i.e., Damon-Eshbach-like modes (n DE) characterized by n nodal surfaces nearly parallel to the static magnetization and backwardlike modes (m BA) with m nodal surfaces nearly perpendicular to the static magnetization.[8] The mode without nodes (quasiuniform) is the fundamental (F). These "bulk" modes contribute to the BLS spectra with the most intense peaks. In Fig. 2 the frequency curves of five calculated modes of this family are drawn corresponding in the order of ascending frequency to the 4-BA and 2-BA modes, the F mode, the 2-BA×1-DE mixed mode, and the 1-DE mode. The submicrometric size of the rings guarantees the coherence of these quantized spin modes differently from the partial decoherence found in micrometric rings.[10] (ii) Modes localized close to the upper ($\phi\approx\pi/2$) and lower ($\phi\approx3\pi/2$) sectors of the ring where the internal magnetic field $\boldsymbol{H}_i$ is inhomogeneous. Each of these sectors can accommodate several kinds of excitations. First, we have modes similar to those previously described, i.e., with nodal surfaces either parallel or perpendicular to the magnetization. Therefore we have Damon-Eshbach-like modes with n nodes in the upper/lower sectors called "n-DE-loc" and backwardlike modes with m nodes called "m-BA-loc." There is also a nodeless mode localized in these sectors called F-loc observed experimentally and already investigated in a previous work.[8] Finally, there are excitations [called end modes (EM)] localized at the inner and outer borders of the ring in the direction of the applied field. All these modes may be S or AS according to the definition given in Sec. II giving rise to degenerate doublets as the upper and lower sectors are far enough to nearly decouple the precessional motion in the two regions. A few modes of the onion state described here have been also observed in larger rings (2 μm wide) by broadband spin-wave spectroscopy.[9] Apart from the different nomenclature, the mode profiles and their localization seem to coincide with our results.

The nature of modes existing in the onion state can be better understood looking at the spatial distribution of the component of the internal magnetic field (H_{iy}) along the direction of the applied field. This is shown in panel (a) of Fig. 3, which clearly exhibits two regions ($\phi\approx\pi$, 2π), where $\boldsymbol{H}_i$ is approximately constant and nearly equal to the applied field (−440 Oe) that accommodate the "bulk" modes described in point (i), and a complex double-well structure in the upper and lower sectors of the ring ($\phi\approx\pi/2$, $3\pi/2$) caused by the curled magnetization of the onion state close to the ends of the dot, which houses the variety of "localized" excitations of point (ii).

The profiles of the F-loc modes are shown in Fig. 4 for both members of the doublet. The BLS cross section is appreciable for the S mode and vanishes for the AS mode because in the latter case the out-of-phase precessions on the two sides of the $(x$-$z)$ scattering plane cancel out in the scattering amplitude.[21] The measured frequency of these S F-loc

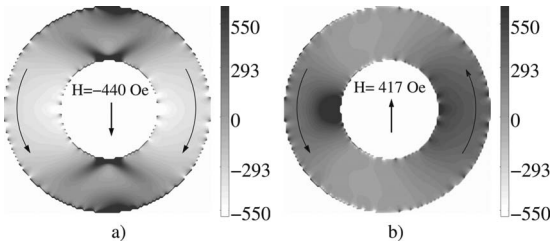

FIG. 3. The y component H_{iy} of the internal magnetic field represented in grayscale (Oe). Left-hand side: onion state for an applied field $H=-440$ Oe. Right-hand side: vortex state for $H=417$ Oe. The y axis points upward.

modes is well reproduced by the DMM calculations as can be seen in Fig. 2. In the field range from −430 to 110 Oe, the onion state is distorted (phases II and III) and the cross section fades so that the experimental points are broadened and are less intense. The DE-loc and BA-loc modes present a weak scattering strength and are not observed in the spectra although they appear among the calculated normal modes.[22]

The EMs are very interesting because they occur in a quartet and may trigger magnetic phase transitions. In Fig. 5 we illustrate the four combinations of S or AS character and of possible localization at the inner or outer borders of the ring. The S and AS doublets (on the same rows in Fig. 5) are degenerate, while the inner/outer doublets (on the same columns in Fig. 5) have slightly different frequencies because the two ring borders are not equivalent. As a matter of fact the outer localization of modes in panels (a) and (b) of Fig. 5 implies a smaller frequency. It is interesting to note that the localization of the EMs almost exactly coincides with the deep minima of the internal field, i.e., "black" regions where the internal field is antiparallel to the applied field as shown in the left-hand panel of Fig. 3. From this point of view these EMs of the ring are the analogous of the EMs of elongated particles.[1,15] Note that the inner EMs present a major localization in a V-shape region according to the form of the minima of the internal field emerging from the inner border. The relevance of the EMs in triggering the onion-to-vortex transition will be discussed in Sec. IV. The EMs have not been observed in the BLS spectra because of the small scattering cross section associated with the limited extension of the mode localization and to the broadening effect on the measured BLS peaks caused by the dispersion of the ring shape over the array.

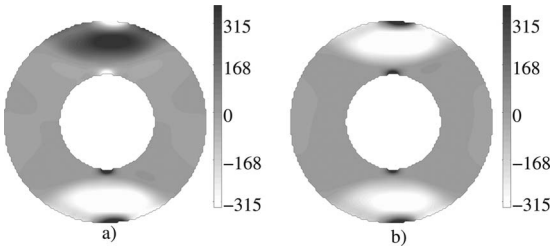

FIG. 4. Calculated (normal) z component of the dynamic magnetization of the (a) antisymmetric and (b) symmetric F-loc modes localized in the upper and lower sectors of the ring. The dynamic magnetization is represented in grayscale (arbitrary units). The dot is in the onion state and $H=-440$ Oe (directed downwards).

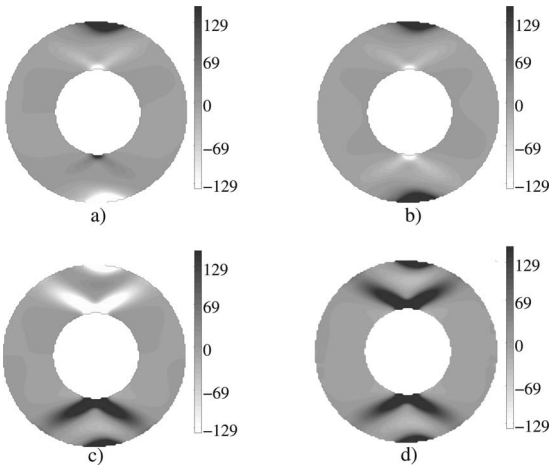

FIG. 5. Calculated (normal) z component of the dynamic magnetization of the four end modes. (a) AS outer EM, (b) S outer EM, (c) AS inner EM, and (d) S inner EM. The dynamic magnetization is represented in grayscale (arbitrary units). The dot is in the onion state and $H=-440$ Oe (directed downwards). "Outer" modes are mainly localized close to the external border of the ring. "Inner" modes are mainly localized close to the internal border with a V-shape pattern.

B. Magnetic vortex phase

The modes of the vortex state can be classified according to the standard notation (m,n) used for disks[23] in terms of a radial index n and an azimuthal index m. In particular in a perfect ring there are axially symmetric modes $(0,n)$ and azimuthal modes $(\pm m,0)$ occurring in doublets. Although the ring we used for the calculations is asymmetric in principle, it is meaningful to keep using this nomenclature because of the very small degree of asymmetry. The main properties of these modes have been discussed in detail in Ref. 8 in the field range $(0,\ H_{c2})$ and here are only summarized in order to understand the evolution of the modes as function of the applied field between H_{c1} and H_{c2} shown in Fig. 2.

Each axially symmetric mode $(0,n)$ splits into two modes as soon as the Zeeman field is switched on, essentially because the internal field is different in the two arms of the ring as shown in Fig. 3(b). One of these modes labeled $(0,n\ \ \pi)$ is localized in the left arm $(\phi\approx\pi)$ and its frequency decreases vs the applied field; the other mode labeled $(0,n\ \ 2\pi)$ is localized in the right arm $(\phi\approx 2\pi)$ and its frequency increases vs the applied field. This feature is illustrated in Fig. 2 for the modes (0,1). We notice that for both these modes the frequency dependence on the applied field is almost linear.

In axially symmetric rings due to the physical absence of the vortex core, the $(\pm m,0)$ azimuthal doublets are degenerate in frequency when $H=0$ (Ref. 23) but split in an external field. However this splitting is not observed in BLS spectra because one of the modes is not Brillouin active, at least in our scattering geometry; therefore only the calculated active modes $(+m,0)$ are shown in Fig. 2. The localization of the azimuthal modes vs the applied field is peculiar. The F mode and the low index modes $(m,0)$ with $m=1$, 2, and 3 localize in the arm of the ring where the magnetization is aligned with the applied field (right arm in our case),[8] while the

lowest frequency modes with m in the range between 4 and 9 localize in the opposite arm.[22] Also the slope of the frequency evolution with the field intensity is different: the former modes exhibit a positive slope, the latter modes a negative slope. This feature is shown in Fig. 2, where it can be noted in particular that the frequency of the (6,0) mode vanishes at the critical field H_{c2}. The relationship between the soft-mode behavior and the vortex-to-onion state transition will be discussed in Sec. IV. Note that the dispersion of the (3,0) and (4,0) modes has been changed with respect to that drawn in Fig. 2 of Ref. 8 thanks to a better assignment. In fact, several azimuthal modes are present in the range 5–8 GHz, although not shown for simplicity in Fig. 2, and the assignment needs great care due to the hybridization effects that mix up the modes when H varies. There are other generally small differences between the calculated curves of Fig. 2 and those of Ref. 8 due to the small shift of the hollow of the ring implemented in the present work.

IV. SOFT MODES AND MAGNETIC PHASE TRANSITIONS

We have already remarked that in our micromagnetic calculations of the equilibrium states the symmetry of the magnetization field $\boldsymbol{M}$ with respect to the x-z mirror plane is conserved. This is imposed by the shape of the asymmetric ring and by its relationship with the direction of the applied field. First-order magnetic phase transitions are marked by a discontinuity of the total magnetization of the dot. We have found that there is a correspondence between these discontinuities and those in the frequencies of the modes. In addition, on one side of the transition, a mode becomes soft, i.e., reaches zero frequency. We have already remarked that the two small discontinuities of the magnetization and the related soft modes for $H=-430$ and -48 Oe are artifacts. Instead, there is experimental evidence of the existence of the other two transitions from onion-to-vortex states and from vortex-to-reversed-onion states, so that it is meaningful to study the relationship between these transitions and the modes softening, at least from the point of view of the calculation. In fact there is no direct experimental signature in the BLS data reported in Fig. 2 of the presence of modes below about 3 GHz.

The critical field H_{c1} marks the onion-to-vortex states transition. The equilibrium state of the magnetization and the spatial profile of the soft AS-EM just before the transition ($H \approx 110$ Oe) are shown in the upper row of Fig. 6 in panels (a) and (b), respectively. This soft mode corresponds (by frequency continuity) to the outer AS-EM given in Fig. 5(a) for a different field. Note that the increased field induces a strong distortion of the equilibrium state [Fig. 6(a)] and consequently a change in the soft-mode profile so that the localization of this mode is distributed in narrow stripes across the width of the ring. At the critical field H_{c1} there are no restoring "forces" with respect to the precession represented by the soft mode;[13] therefore the system becomes unstable in the limited area where the amplitude of the soft mode is large and follows a path in the phase space that initially is given by a new (unstable) state obtained by summing the perturbation [dynamic magnetization of Fig. 6(b)] to the initial state

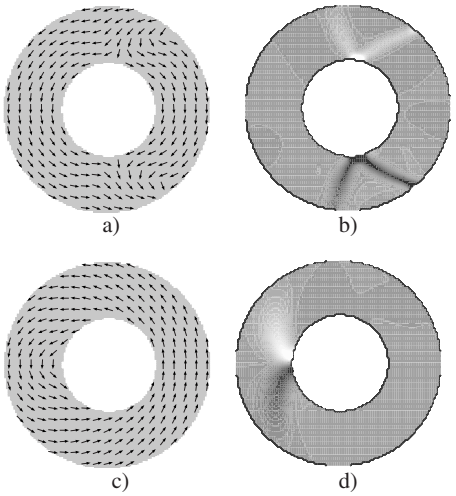

FIG. 6. Magnetic equilibrium configuration [(a) and (c)] and x component of the dynamic magnetization of the corresponding soft modes [(b) and (d)] just before the phase transitions. The upper row refers to $H=110$ Oe (before the onion-to-vortex transition), the lower row refers to $H=417$ Oe (before the vortex-to-onion transition). The dynamic magnetization is represented in grayscale (arbitrary units). The applied field H is directed upwards.

[Fig. 6(a)]. By accurate inspection of these figures, the effect of the perturbation corresponds to nucleation of two anticlockwise vortices at the outer border of the ring approximately for $\phi \approx \pm \pi/3$. Note that the perturbation has vector character; in Fig. 6(b) only the x component is reported, the other in-plane y component is similar to the x component but is S instead of AS. Therefore the soft mode triggers the onset of the instability that immediately afterward propagates through the whole ring and produces the macroscopic transition to a new equilibrium state. Obviously our linear dynamics treatment is meaningful only at the onset of the transition; but it is in agreement with the time behavior provided by the micromagnetic simulator OOMMF, which actually indicates the formation of two "local" vortices that move toward the ring center, annihilate, and produce the magnetization reversal in the right arm of the ring of Fig. 6(a). In this way the "global" vortex state is formed. Note that the global vortex chirality is univocally determined by the asymmetry of the ring.[24] In our case, in naive terms, the right arm of the ring is narrower than the left arm and therefore it reverses first in an opposite applied field due to the smaller energy cost; an anticlockwise vortex is therefore nucleated. Our theoretical analysis allows for deeper insight: The axial symmetry breaking due to the displacement of the hollow produces an asymmetric (with respect to the normal to the displacement) internal field and a soft mode mainly localized in the right arm of the ring as in Fig. 6(b). Therefore the soft mode is responsible for the nucleation of two anticlockwise (unstable) vortices in that arm and eventually for the reversal of the magnetization. Very interestingly, this "dynamic picture" leads to the same results and is complementary to an "energetic picture" recently proposed.[25]

A similar explanation applies to the vortex-to-onion transition occurring at the critical field H_{c2}. In this case the (6,0) azimuthal mode goes soft according to Fig. 2. The precession

amplitude of the soft mode immediately before the critical field given in Fig. 6(d) is AS and it is large only close to $\phi=\pi$ as already remarked in Sec. III B. It is amazing that the Zeeman field produces such a strong localization of the (6,0) mode, which at the transition presents a profile completely unexpected for an azimuthal mode.[8] This localization occurs in the left arm of the ring where the internal field H_{iy} [Fig. 3(b)] is characterized by large positive values. Here the internal field is antiparallel to the magnetization shown in Fig. 6(c). Applying the same arguments suggested for the H_{c1} transition, the soft mode induces the nucleation of a single vortex at the inner border close to $\phi=\pi$. The time evolution of the system provided by OOMMF envisages that the vortex moves to the left and finally annihilates at the outer border leaving behind a magnetization pointing upward: therefore, the reversed-onion state is generated. A few experimental points in Fig. 2 close to $H=200$ Oe seem to validate the calculated softening of the (6,0) mode; however they are too far from the critical field to draw a final conclusion. More sensitivity to the low-frequency localized soft mode is required and therefore spatially resolved microfocused BLS investigation could clarify this point.

The existence of a soft mode in the vortex-to-onion transition has also been recently predicted in microwave-assisted switching of micrometric rings.[26] In particular these authors found: (i) a few distinct resonances due to azimuthal excitations (called I_n) corresponding to our (3,0) and (4,0) modes with a field dispersion of negative slope and responsible for the microwave-assisted reversal; (ii) a low-frequency mode envisaged as a soft mode, which could correspond to our (6,0) mode. However the interpretation of this soft mode and of its localization is different. In Ref. 26 it is supposed that the soft mode is an edge mode localized in the direction of the applied field, while we have found as explained above that it is localized in the arm of the ring where the magnetization is oriented antiparallel to $\boldsymbol{H}$.

V. CONCLUSIONS

In this paper, we have shown that BLS provides a lot of information about the spin excitations of a magnetic nanoring throughout a hysteresis cycle that leads to magnetization reversal of the rings, starting from an almost saturated onion state, reaching the vortex state and eventually the final reversed-onion state. The intriguing complexity of the spectra can be explained by comparison with micromagnetic calculations performed directly in the frequency domain. The dynamical matrix method, which provides both the frequencies and the dynamic magnetization profiles of the spin modes, has been used to this purpose. The spin mode calculations reproduce with good accuracy all the modes present in the BLS spectra (frequency greater than about 3 GHz) so that we can analyze with confidence also the modes calculated below this frequency. The calculations show that there exist low-frequency modes localized in confined regions of the rings reaching zero frequency at the critical fields where first-order magnetic transitions occur. We have identified the soft modes responsible for the onion-to-vortex and the vortex-to-reversed-onion transitions.

At a critical field there are no restoring "forces" contrasting the precession magnitude of the soft mode, the system becomes unstable in the limited area where the amplitude of the soft mode is large and then the instability propagates in the whole magnetic element producing the macroscopic transition to a new equilibrium state. The shape and symmetry of the dynamic magnetization profile of the soft mode provide the initial modifications of the magnetization at the onset of the transitions. We have actually found for the two transitions considered here that the perturbation induced on the ground state by the soft mode triggers the same modifications of the magnetization that can be found in conventional micromagnetic simulations in time domain, which integrate the equations of motion of the magnetization.

ACKNOWLEDGMENT

Support by the PRIN Grant No. 2007X3Y2Y2 of Ministero Istruzione, Università e Ricerca is acknowledged.

[1] C. Bayer, J. Jorzick, S. O. Demokritov, A. N. Slavin, K. Y. Guslienko, D. V. Berkov, N. L. Gorn, M. P. Kostylev, and B. Hillebrands, in *Spin Dynamics in Confined Magnetic Structures III*, edited by B. Hillebrands and A. Thiaville (Springer, Berlin, 2006), pp. 57–103.

[2] C. Mathieu, J. Jorzick, A. Frank, S. O. Demokritov, A. N. Slavin, B. Hillebrands, B. Bartenlian, C. Chappert, D. Decanini, F. Rousseaux, and E. Cambril, Phys. Rev. Lett. **81**, 3968 (1998).

[3] Xiaobin Zhu, Marek Malac, Zhigang Liu, Hui Qian, Vitali Metlushko, and Mark R. Freeman, Appl. Phys. Lett. **86**, 262502 (2005).

[4] F. Giesen, J. Podbielski, T. Korn, M. Steiner, A. van Staa, and D. Grundler, Appl. Phys. Lett. **86**, 112510 (2005).

[5] I. Neudecker, M. Kläui, K. Perzlmaier, D. Backes, L. J. Heyderman, C. A. F. Vaz, J. A. C. Bland, U. Rüdiger, and C. H. Back, Phys. Rev. Lett. **96**, 057207 (2006).

[6] J. Podbielski, F. Giesen, and D. Grundler, Phys. Rev. Lett. **96**, 167207 (2006).

[7] X. Zhu, Z. Liu, V. Metlushko, L. Giovannini, F. Montoncello, F. Nizzoli, and M. R. Freeman, J. Appl. Phys. **99**, 08F307 (2006).

[8] G. Gubbiotti, M. Madami, S. Tacchi, G. Carlotti, H. Tanigawa, T. Ono, L. Giovannini, F. Montoncello, and F. Nizzoli, Phys. Rev. Lett. **97**, 247203 (2006).

[9] F. Giesen, J. Podbielski, and D. Grundler, Phys. Rev. B **76**, 014431 (2007).

[10] H. Schultheiss, S. Schäfer, P. Candeloro, B. Leven, B. Hillebrands, and A. N. Slavin, Phys. Rev. Lett. **100**, 047204 (2008).

[11] M. Kläui, C. A. F. Vaz, L. Lopez-Diaz, and J. A. C. Bland, J. Phys.: Condens. Matter **15**, R985 (2003).

[12] F. Montoncello, L. Giovannini, F. Nizzoli, P. Vavassori, M. Grimsditch, T. Ono, G. Gubbiotti, S. Tacchi, and G. Carlotti, Phys. Rev. B **76**, 024426 (2007).

[13] G. Gubbiotti, M. Madami, S. Tacchi, G. Carlotti, M. Pasquale, N. Singh, S. Goolaup, and A. O. Adeyeye, J. Phys.: Condens. Matter **19**, 406229 (2007).
[14] F. Montoncello, L. Giovannini, F. Nizzoli, P. Vavassori, and M. Grimsditch, Phys. Rev. B **77**, 214402 (2008).
[15] M. Grimsditch, L. Giovannini, F. Montoncello, F. Nizzoli, G. K. Leaf, and H. G. Kaper, Phys. Rev. B **70**, 054409 (2004).
[16] L. Giovannini, F. Montoncello, F. Nizzoli, G. Gubbiotti, G. Carlotti, T. Okuno, T. Shinjo, and M. Grimsditch, Phys. Rev. B **70**, 172404 (2004).
[17] F. Montoncello and F. Nizzoli, in *Magnetic Properties of Laterally Confined Nanometric Structures*, edited by G. Gubbiotti (Transworld Research Network, Kerala, India, 2006), pp. 131–165.
[18] In the previous paper on the subject (Ref. 8) it was used a cell size $5\times5\times20$ nm^3. Here it has been adopted a slightly larger cell size to speed up calculations, after verification that the numerical results are practically the same.
[19] M. J. Donahue and D. G. Porter, *OOMMF User's Guide, Version 1.0* (NIST, Gaithersburg, MD, 1999).
[20] J. R. Sandercock, in *Light Scattering in Solids III*, edited by M. Cardona and G. Güntherodt (Springer, Berlin, 1982), p. 173.
[21] G. Gubbiotti, G. Carlotti, T. Okuno, M. Grimsditch, L. Giovannini, F. Montoncello, and F. Nizzoli, Phys. Rev. B **72**, 184419 (2005).
[22] F. Montoncello, L. Giovannini, and F. Nizzoli, J. Appl. Phys. **103**, 083910 (2008).
[23] B. A. Ivanov and C. E. Zaspel, Appl. Phys. Lett. **81**, 1261 (2002).
[24] F. Giesen, J. Podbielski, B. Botters, and D. Grundler, Phys. Rev. B **75**, 184428 (2007).
[25] S. Prosandeev, I. Ponomareva, I. Kornev, and L. Bellaiche, Phys. Rev. Lett. **100**, 047201 (2008).
[26] J. Podbielski, D. Heitmann, and D. Grundler, Phys. Rev. Lett. **99**, 207202 (2007).